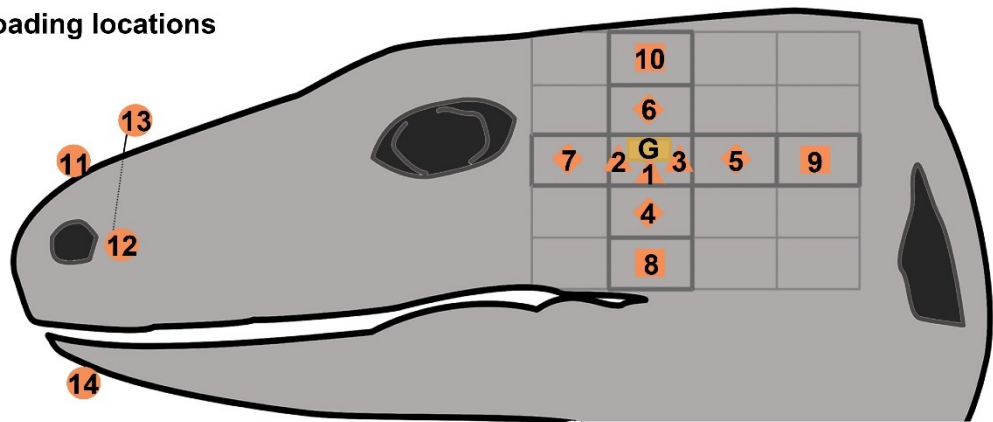


Fig. S1. 'Perpendicular Tensile' test experiment. A. Schematic representation of the 'Perpendicular Tensile' test experiment. B. Waveforms recorded from the external and internal sides of the osteoderms using single element gauges. The grey area highlights the time period during which the osteoderm was loaded. ES: external side of the dissected osteoderm. IS: internal side of the dissected osteoderm. OD: osteoderm. SG: single element gauge. C. Tensile and compressive strains recorded from a subsample of dissected ODs. Here, the OD was loaded perpendicular to its long axis using different weights (100, 200, 500g) and strains were recorded along that axis using single strain gauges placed on the external and internal sides of the OD. *Co.z.*: *Corucia zebrata*. *He.h.*: *Heloderma horridum*. *Ti.r.*: *Tiliqua rugosa*. *Ti.s.*: *Tiliqua scincoides*.

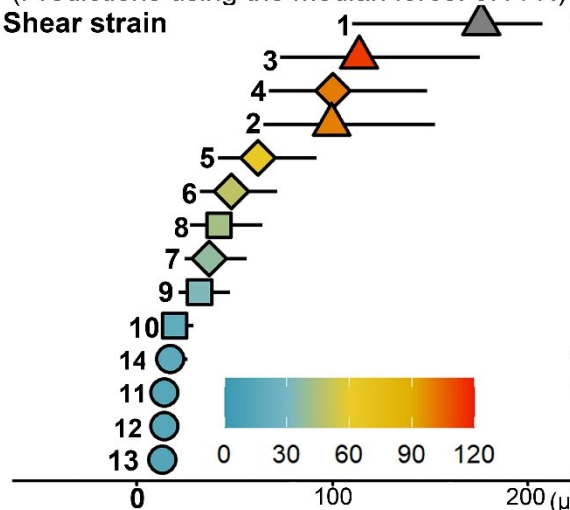
A. Gage and loading locations



B. Dynamic loading

(Predictions using the median force: 0.44 N)

Shear strain



C. Static loading

(Predictions using the median force: 8 N)

Shear strain

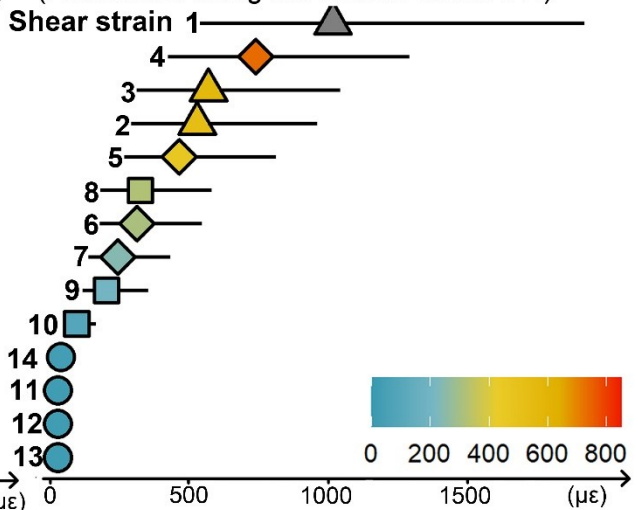


Fig. S2. Effect of the location of the loading on the shear strains predicted for the instrumented osteoderm. A. Location of the 14 different places where loading was applied. Locations are indicated by a triangle when force is applied directly on the instrumented osteoderm, a diamond when the force is applied on an osteoderm adjacent to the instrumented osteoderm, a square when it is applied to an osteoderm separated from the instrumented osteoderm by one osteoderm, and a circle when it is applied near the rostral end of the head. B. Shear strains predicted for each location by the Linear Mixed Model obtained using the ‘dynamic’ data. C. Shear strains predicted for each location by the Linear Mixed Model obtained using the ‘static’ data.

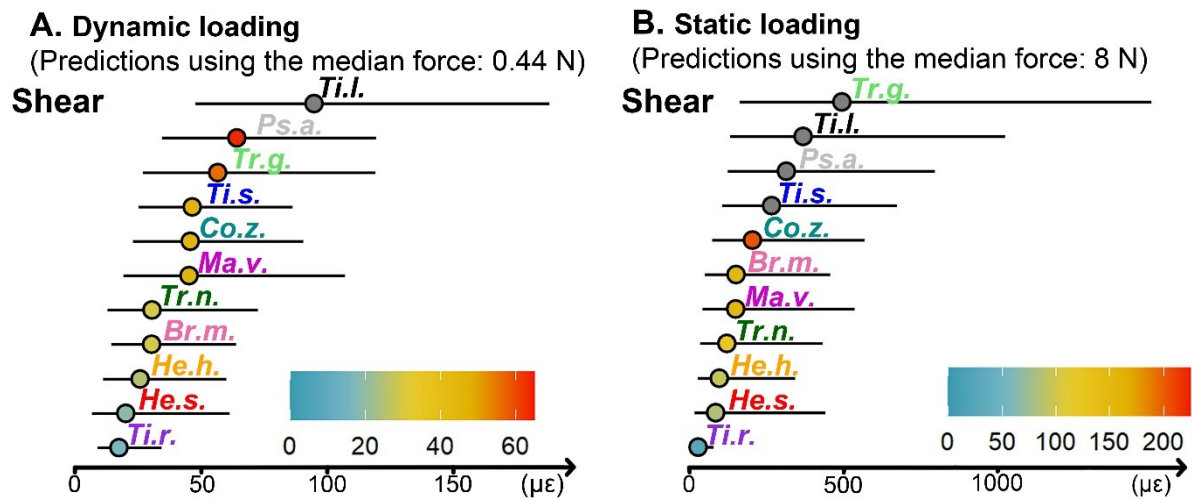


Fig. S3. In-toto interspecific differences in the stiffness of the skin system. The graphs show the shear strains predicted by the Linear Mixed Model for the instrumented osteoderm. All the locations were included in the model. *Br.m.*: *Broadleysaurus major*. *Co.z.*: *Corucia zebrata*. *He.h.*: *Heloderma horridum*. *He.s.*: *Heloderma suspectum*. *Ma.v.*: *Matobosaurus validus*. *Ps.a.*: *Pseudopus apodus*. *Ti.r.*: *Tiliqua rugosa*. *Ti.s.*: *Tiliqua scincoides*. *Ti.l.*: *Timon lepidus*. *Tr.g.*: *Tribolonotus gracilis*. *Tr.n.*: *Tribolonotus novaeguineae*.

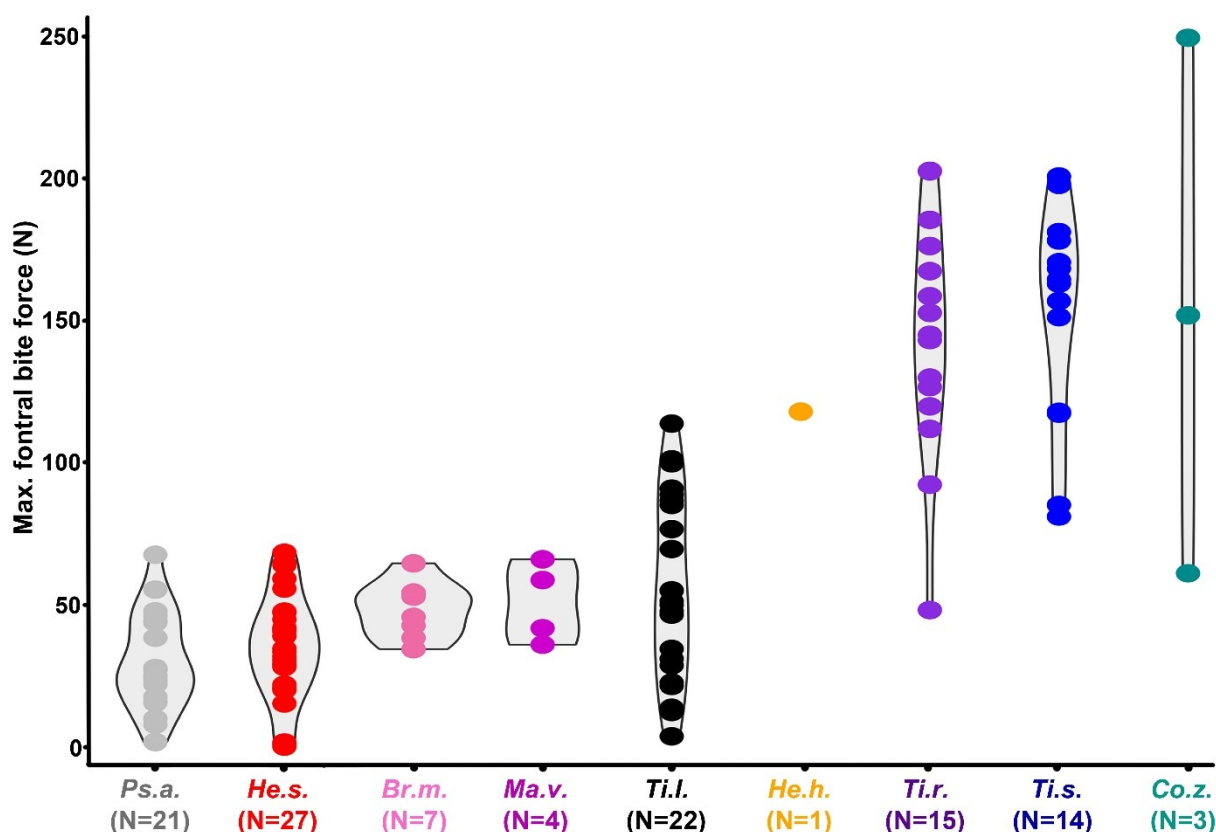


Fig. S4. Interspecific differences in the maximal bite force. Violin plots showing bite forces measured at the anterior end of the mouth for eight lizard species studied in this paper. Data are from a dataset from A. Herrel and were collected following the procedure described in Herrel *et al.* (1999). *Br.m.*: *Broadleysaurus major*. *Co.z.*: *Corucia zebrata*. *He.s.*: *Heloderma suspectum*. *He.s.*: *Heloderma suspectum*. *Ma.v.*: *Matobosaurus validus*. *Ps.a.*: *Pseudopus apodus*. *Ti.r.*: *Tiliqua rugosa*. *Ti.s.*: *Tiliqua scincoides*. *Ti.l.*: *Timon lepidus*.

Table S1. Analysis of Deviance Table (Type III Wald chi-square tests). Loading Force was log-scaled.

Signif. codes: 0 '***' 0.001 '**' 0.01 '*' 0.05 '.' 0.1 ' ' 1

[Click here to download Table S1](#)

Table S2. Shear (Log-transformed) strains predicted for a dynamic loading of 0.44 N and a static loading of 8 N.

[Click here to download Table S2](#)